

Additive Manufacturing of NASA HR-1 Material for Liquid Rocket Engine Component Applications

Colton Katsarelis, Po Chen, Paul Gradl, Chris Protz, Zachary Jones
NASA Marshall Space Flight Center, Huntsville, AL 35812

David Ellis, Laura Evans
NASA Glenn Research Center, Cleveland, OH 44135

ABSTRACT

NASA HR-1 is a high-strength Fe-Ni superalloy designed to resist high pressure, hydrogen environment embrittlement, oxidation, and corrosion. NASA HR-1 was originally developed at NASA in the 1990's and derived from JBK-75 to increase strength and ductility in high-pressure hydrogen environments. The NASA HR-1 chemistry was formulated to meet requirements for liquid rocket engine applications, specifically components used in a high-pressure hydrogen environment. Recent developments using additive manufacturing (AM) have made this material an attractive option for channel-cooled nozzles under the Rapid Analysis and Manufacturing Propulsion Technology (RAMPT) program and other liquid rocket engine component applications. The RAMPT program has baselined to fully evolve and characterize NASA HR-1 material. NASA HR-1 meets materials requirements for liquid rocket engine components, including good hydrogen resistance, high conductivity, good low cycle fatigue performance, and high elongation and strength for channel-cooled nozzles in high heat flux environments. Initial development and characterization has been completed using blown powder Directed Energy Deposition (DED) and Laser Powder Bed Fusion (L-PBF) additive manufacturing techniques to develop material test samples and nozzle hardware. NASA HR-1 powder has been sourced and characterized from several powder suppliers, and a series of development and hardware samples completed fabrication using DED and L-PBF. Characterization of the material has included heat treatment development, metallography, chemistry evaluations, mechanical testing, measurement of thermophysical properties, and fabrication of relevant nozzle hardware to demonstrate feasibility. This paper presents results from the process and early materials development and provide future development work including hardware fabrication.

INTRODUCTION

High-pressure, high-temperature liquid rocket engine (LRE) components provide an extreme and challenging environment for any material. The complexities of these components, in particular regeneratively-cooled nozzles, are numerous since these are often large scale component structures that require very thin-walls for the channels and extreme environments providing challenging thermal and structural loads. Complicated with the challenging thermal and structural loads are the propellants used for cooling and the combustion process. Liquid and gaseous hydrogen propellant offers additional challenges for materials that must resist Hydrogen Environment Embrittlement (HEE). Based on these environments, a regeneratively-cooled nozzle has key requirements that must be considered for material selection:

- **Thermal Conductivity** – A primary driver of wall temperature in regenerative-cooling is conduction through ribs and the hotwall; a higher thermal conductivity is required to maintain positive structural margins.
- **Low Cycle Fatigue (LCF)** – A nozzle must go through several cycles including start-up and shutdown transients that drive loads locally on the hotwall and globally such as sideloads. High strains on the hotwall with fully reversal strains are a driver of multiple cycles.
- **Yield Strength** – High strength is required to react loads from internal pressures, transient side loads, and thrust chamber assembly thrust loads

- **Elongation** – Ductility is important due to high strains in the nozzle, both locally (hotwall, channels, backside walls) and globally
- **Hydrogen Embrittlement** – Material will be used in a high-pressure hydrogen environment since hydrogen is coolant in nozzle, so ductility and resistance important.

While a few materials are available to meet these requirements, there are trades that must be made amongst the various properties during operation, which could make the design heavier than necessary or lead to premature failure due to low margins. Aerospace structural alloys that encounter gaseous hydrogen in operation (for example, hot gas manifolds in a rocket engine and hotwall of a rocket nozzle) require adequate resistance to HEE in addition to good strength and oxidation/ corrosion resistance. Austenitic stainless steels, A-286 and JBK-75 are commonly used in such applications. However, these alloys have their limitations. Austenitic stainless steels (such as 304, 310, and 316) are hydrogen-resistant, but have low yield strength (around 276 MPa). Fe-base superalloys that are derived from austenitic stainless steels (such as A-286, and JBK-75) have adequate resistance to HEE, corrosion, and oxidation, but lack high strength. In consideration of these problems, NASA HR-1 was specifically developed [1] as a higher strength structural alloy that has combined virtues of HEE, oxidation, and corrosion resistance.

One important fact that clearly emerges from literature review is that the hydrogen-resistant Fe-base superalloys, such as A-286, JBK-75 [2], have γ -matrix compositions evolving from hydrogen-resistant stainless steels (single γ -phase materials). To expedite the development of a higher strength HEE resistant Fe-Ni-based superalloy, the alloy design for NASA HR-1 was approached by formulating a hydrogen-resistant γ -matrix that resembles JBK-75 along with increasing γ' volume fraction and strengthening γ -matrix. The matrix phase, γ , is a solid solution of Fe, Ni, Co, Cr, Mo, W, and V. Whereas the precipitate phase γ' is composed of hardening elements Ti and Al. Another phase observed in the microstructure is the η -phase, which is a Ti-rich acicular precipitate that generally forms at the grain boundaries under certain heat-treated conditions, and it forms within the grains after prolonged exposure to elevated temperatures.

The γ' volume fraction was increased by adding more γ' -forming elements (Ti and Al), but excessive additions could lead to super-saturation of the γ matrix, resulting in extensive grain-boundary η -phase precipitation and ductility loss in hydrogen [3, 4]. Therefore, improved solid solubility had to be obtained for the γ' forming elements, requiring a matrix with higher levels of Ni and/or Co. Strengthening of γ -matrix was achieved by increasing Mo and adding W. W and Mo are very potent solid-solution hardeners in Ni-base superalloys [5, 6]. Tungsten, which was reportedly having retarding effects on η -phase precipitation, was added to stabilize the grain boundaries [7]. Mn and Si were excluded for NASA HR-1, due to weldability concerns [2].

PHACOMP (Phase Computation) analysis was used for NASA HR-1 development to evaluate the phase stability of the experimental alloys [8]. This concept was devised based on molecular orbital calculation (the discrete variational (DX)- $X\alpha$ cluster method) for transition-metal-based alloys. The primary parameter used is the d-orbital energy level (Md) of alloying transition metal elements. Md denotes the d-orbital energy above the Fermi energy level for the transition metals. Md has been used to estimate the solubility limit of the terminal solid solution in transition-metal-based alloys [8–10]. The PHACOMP value Md for NASA HR-1 was kept close to that of JBK-75 to maintain γ -matrix stability and minimize η precipitation. Table 1 shows the nominal chemical composition of NASA HR-1, JBK-75, and A-286.

In brief, the alloy chemistry rationale for NASA HR-1 follows the following criteria:

- The Fe:Ni ratio was varied to improve solid solubility and to identify HEE-resistant compositional ranges. Higher Ni can reduce solidification and HAZ cracking susceptibility [1,11].
- Volume fraction of γ' was increased by adding more Ti and Al for higher strength.
- Co was added to reduce Md value so that the Fe:Ni ratio can be kept close to that of JBK-75.
- W was added to strengthen the γ -matrix and to retard η precipitation in the grain boundaries [6, 7].
- Mo content was increased to 2.0% to strengthen the γ -matrix and to reduce solidification and HAZ cracking susceptibility [1,11].

- Cr content was kept at 14.0 -16.0 percent to preserve corrosion/oxidation resistance.
- V was kept at the same level as JBK-75 to improve resistance to notch effect and hot formability.

Table 1: Nominal compositions of A286, JBK-75, and NASA HR-1

	A-286	JBK-75	NASA HR-1
Fe	Balance	Balance	Balance
Ni	25.5	30	34
Co	-	-	3.3
Cr	14.8	14.8	15
Mo	1.3	1.3	2
V	0.3	0.3	0.3
W	-	-	1.8
Ti	2.1	2.2	2.5
Al	0.2	0.3	0.3

NASA HR-1 is potentially an enabling material for use in high-pressure, high temperature hydrogen-based liquid rocket engine components. However, the existing vacuum induction melting/vacuum arc remelt (VIM/VAR) processing and supply chain would not support cost trades and alternate fabrication methods would have to be explored. Additive manufacturing technologies provided a critical method for fabrication the NASA HR-1 affordably and a simplified powder and fabrication supply chain. NASA started exploring alternate additive manufacturing technology as part of the MSFC Liquid Engines Office (LEO) Technology Development and under the Rapid Analysis and Manufacturing Propulsion Technology (RAMPT) project using the NASA HR-1 material for channel wall nozzles. Two additive manufacturing technologies are being explored including Laser Powder Bed Fusion (L-PBF) and blown powder directed energy deposition (DED). DED has the ability to produce much larger components than L-PBF.

The blown powder directed energy deposition (DED) process can form near-net shape blanks, final-shape components, and integral channels and features within components providing the ability to significantly reduce part count and eliminate many of the process steps typically required for forming the liner, channel slotting and closeout of the coolant channels for nozzles. This alternative technology is very attractive for these reasons, but at a lower technology readiness level (TRL). NASA's goal was to evaluate the DED technology and mature the process for integral channel wall nozzles, material characterization and properties, design for DED additive manufacturing, and complete hot-fire testing in relevant environments.

The DED process is being studied for several applications of regen-cooled nozzles. This includes forming near-final shape components such as liners, manifolds, and an integrated-channel configuration to minimize part count. A significant advantage of the DED processes is the ability to adapt to a robotic or gantry CNC system with a localized purge or purge chamber, allowing unlimited build volume. Much of the current focus of the DED is being explored to form the entire channel wall nozzle with integral coolant channels within a single AM build. This relies on the DED-fabrication of complex and thin-walled features. Characterization of the material properties produced with this technique is required in order to evolve this process [12].

The blown powder DED fabrication technique uses a coaxial nozzle with a central laser source and powder injected (or blown) into the laser focus. The melt pool is created by the co-axial laser energy source causing a weld bead to be deposited. The powder is accelerated, or blown, into the melt pool using an inert carrier gas to allow for minimal or reduced oxidation in the high temperature deposition/weld. This head system, with integrated focus optics and blown powder nozzle(s), is attached to a robot or gantry system that controls a toolpath defined by the CAD model. The blown powder head can be contained in an inert gas chamber or operated with a local purge. The blown powder system and robot allows complex freeform structures to be built with small integral features, such as thin-walls and

channels. Various optics can be used to vary the laser spot size, and consequently the melt pool width, which control the size of features that can be built. A picture of the process can be seen in Fig 1.

This DED process has several advantages over the L-PBF process, primarily a much larger build volume. The build volume is dictated by the size of the inert gas chamber (build area) or, if built using a local purge, the size of the gantry or robotic system. Powder is only deposited locally and can be fabricated in multi-axis including deposition onto existing features of components. Blown powder is a good trade between high deposition rates and resolution of features, which allows for much higher build rate than L-PBF [13]. The trade of the higher deposition rate is loss of resolution in features such as small holes, channels, wall thicknesses. There are more materials available to select from using the DED process including the ability to fabricate multi-alloys and/or gradient materials [3–5].

Small melting zones can be achieved by controlling the laser parameters. Although features, including wall thicknesses, of less than 0.03” have been produced, a dimension of 0.04” is more realistic with current technology [17,18]. The blown powder deposition technology also has a much rougher surface finish than the powder bed technology. Because of the impact of surface finish on fatigue life, post-processing may be required [19–21].

Prior publications [18,20] discussed specific design details of the blown powder DED process for nozzles and application of the technology to nozzles. A majority of the early blown powder DED evolved the process as a forging or casting replacement technology, such as forming nozzle liners, manifolds, and bimetallic jackets for combustion chambers [22]. This was shown by fabricating large structures and machining to final dimensions. This process has shown a viable option is feasible with acceptable properties.

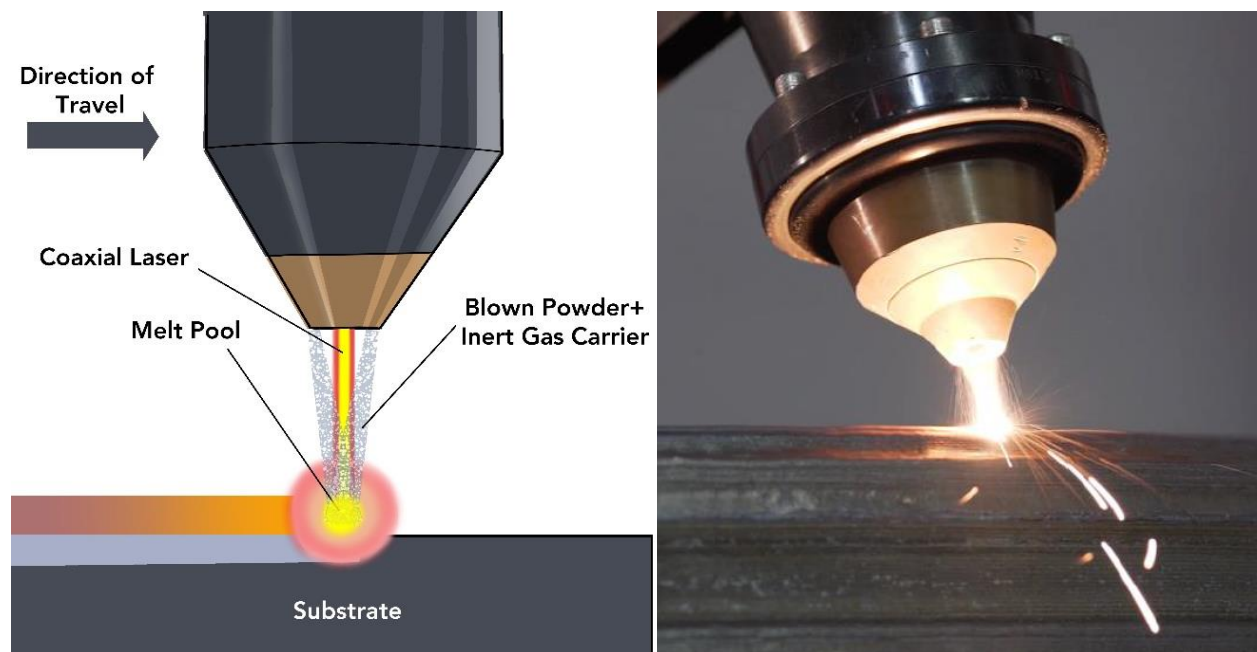


Fig. 1: Overview of Blown Powder DED Process

The current focus of the blown powder DED is on integrated-channel nozzles that can significantly reduce part count and may only require a few post-processing operations to complete an assembly. During this development, several lessons learned were collected on the design process as it relates to DED (compared to previous lessons on L-PBF). Some of the primary differences of DED compared to L-PBF are the inability to use break-away supports, minimum feature size results in thicker as-built walls, feature resolution is more coarse, higher surface roughness, and higher heat input. The integrated-channel nozzle fabrication process (Fig. 2) has rapidly evolved and NASA along with industry partners have demonstrated a variety of initial hardware, including planned hot-fire testing.

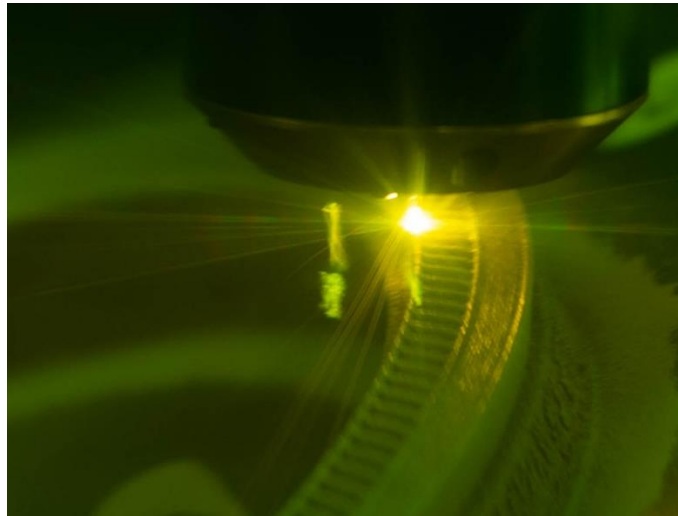


Fig. 2: Blown Powder DED fabrication with integrated channels (RPM Innovations).

The Laser Powder Bed Fusion (L-PBF), or Selective Laser Melting (SLM) has been discussed at length in prior publications [23]. L-PBF is a layer-by-layer additive manufacturing process. The process starts with a 3D-CAD model that is sliced into thin 2D layers that defines the laser toolpath for melting the part. A thin layer of metal powder, typically 30-45 microns, is spread across the build area and a fine focus laser rasters and melts the area that defines the part cross section at that particular layer [21,24]. A build plate is required to initiate the process so the material has something to which it can bond.

After a layer is completed, the build plate is lowered slightly, a new layer of powder is spread, and the laser melts the new build layer. Sufficient power is used to penetrate into previous build layers allowing proper bonding between layers. The process is repeated thousands of times until the part is fully fabricated or grown. This allows the complex internal features to be fabricated, such as the coolant channels. Varying parameters are used for the infill (internal material) and the contouring (surfaces inboard or outboard) for a component.

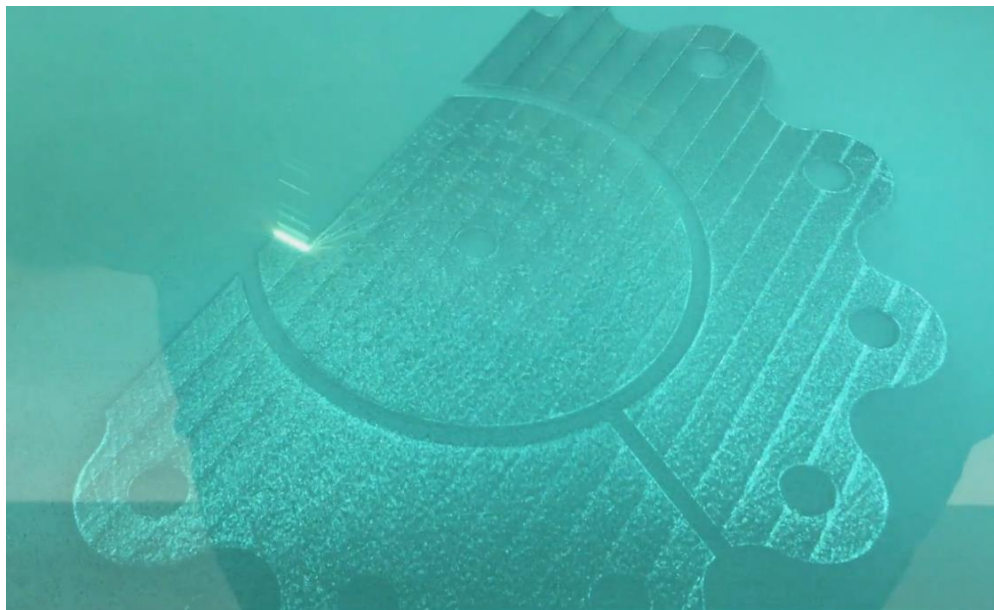


Fig. 3: L-PBF fabrication infill passes for a part

RESULTS AND DISCUSSION

NASA and industry partners completed sets of panels and blocks (Fig. 4) as witness specimens of NASA HR-1 using the DED blown powder deposition process. In addition, small specimens were built using the L-PBF process for comparison. Table 2 shows the compositions, provided by the vendors, of the powders used for these two processes. Specimens were subjected to various heat treatments to examine the evolution of the microstructure and develop a recommended heat treatment for additively manufactured NASA HR-1 parts. Heat treatment evaluation methods included optical microscopy, scanning electron microscopy (SEM), and micro-hardness measurement.

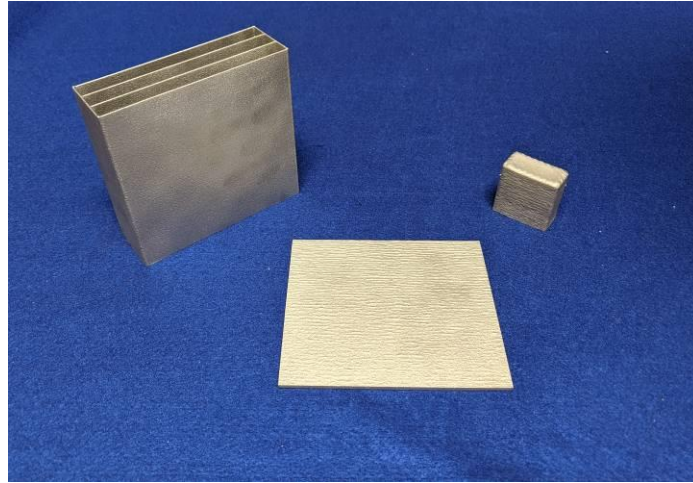


Fig. 4: Blown powder DED NASA HR-1 witness plates (left) and blocks (right) used for materials characterization.

Table 2: Chemical composition of DED cut and SLM cut NASA HR-1 used in this study, provided by the powder vendors.

NASA HR-1 Powder Compositions Wt.%

	DED	SLM
Fe	Bal	Bal
Ni	33.82	34.30
Co	3.45	3.30
Cr	14.61	15.50
Mo	2.32	2.20
V	0.37	0.42
W	1.74	2.00
Ti	2.56	2.50
Al	0.36	0.27

After deposition, parts require several post-processing heat treatment steps in order to attain the materials properties that are desirable for the application. For AM parts, these steps often include a stress relief, homogenization or hot isostatic press (HIP), solution anneal, and aging treatment for precipitation hardened alloys [25]. An effective stress relief mitigates residual stresses built up in the part during deposition and minimizes the potential distortions before further post-processing. The second step, homogenization or HIP, is a treatment performed to promote recrystallization and achieve a uniform equiaxed grain structure in the material. This step is essential to minimize anisotropy in the mechanical properties of the material and to achieve desirable microstructure for welding [26,27]. The third step, solution anneal, brings the part to a solid solution temperature then quenched to maintain that solution. The aging treatment promotes the precipitation of the strengthening phase in the alloy, the γ' phase for NASA HR-1 [1].

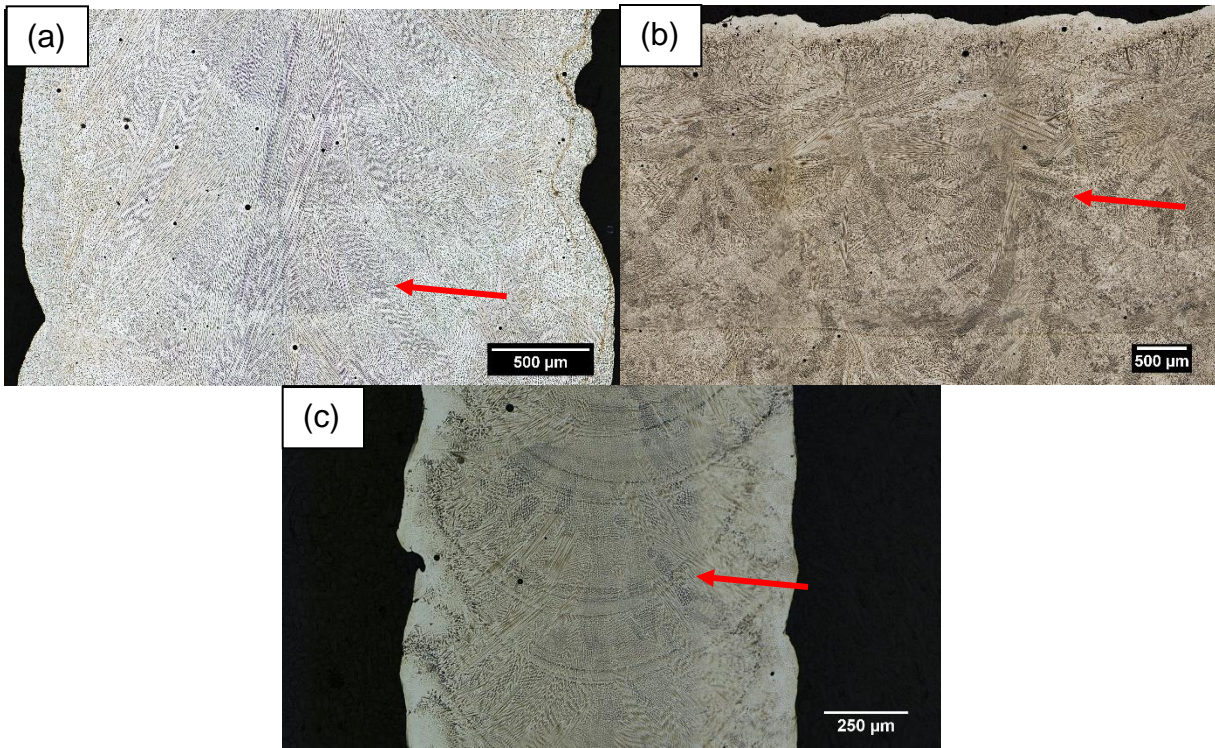


Fig. 5: Optical micrographs of as-built DED NASA HR-1, (a) 3.175 mm single-pass panel; (b) Top Layer Melt Pool of multiple pass block; (c) 1 mm single-pass panel. The red arrows indicate the melt pool boundaries observed in the as-built microstructure.

The DED panels were deposited with a thickness of approximately 3.175 mm for thicker panels and 1 mm for the thin panels. These panels were deposited with single passes per layer that are parallel to the previous layer. The blocks were deposited with a scan strategy where each layer scan is rotated 45° with respect to the previous layer to make a fully dense block. The larger melt pool width was used for both the thick panels and the blocks resulting in large melt pool dimensions in comparison to SLM built specimens. The melt pool boundary is readily apparent in the as built material (Fig. 5). Additionally, large columnar grains had developed branching outward from the center of the melt pool, shown in Fig. 5a and 5b. It was observed that, in panels made with a smaller melt pool width (Fig. 5c), the columnar grains that developed were much smaller than grains in the panels and blocks made with the larger melt pool. Thus, the differences in grain size are likely due to the differences in cooling rates and melt pool dimensions [28]. In the multiple-pass block, smaller grains appeared to develop due to the scan pattern in the block not being parallel in consecutive layers. With each layer, the grain structure breaks-up as the laser scans across the surface melting new material onto the part, and the grains in the new layers do not combine as easily with previous layers since the scan direction changes with each layer. At the top layer of the block, large columnar grains extend from the center of the melt pool similar to the single pass because there was not another layer to help break up the grain structure at all.

Three stress relief temperatures for 1.5 hours were examined to determine an effective stress relief treatment. The temperatures ranged from 926°C (1700°F) to 982°C (1800°F). Fig. 6 shows the microstructure of the HR-1 panels after the various stress relief parameters. At the lowest temperature, the melt pool boundaries were still evident and the dendritic structure in the grains is still distinct. These observations indicate that some recovery had occurred, but the stress relief was not fully effective in mitigating residual stresses. With increasing temperature, the melt pool boundaries dissipated more until they were not evident at the highest temperature. Additionally, the dendritic structure of the grains was not distinct at the highest temperature indicating an effective stress relief. This stress relief cycle of 982°C (1800°F) for 1.5h was the stress relief used on the samples further in the study.

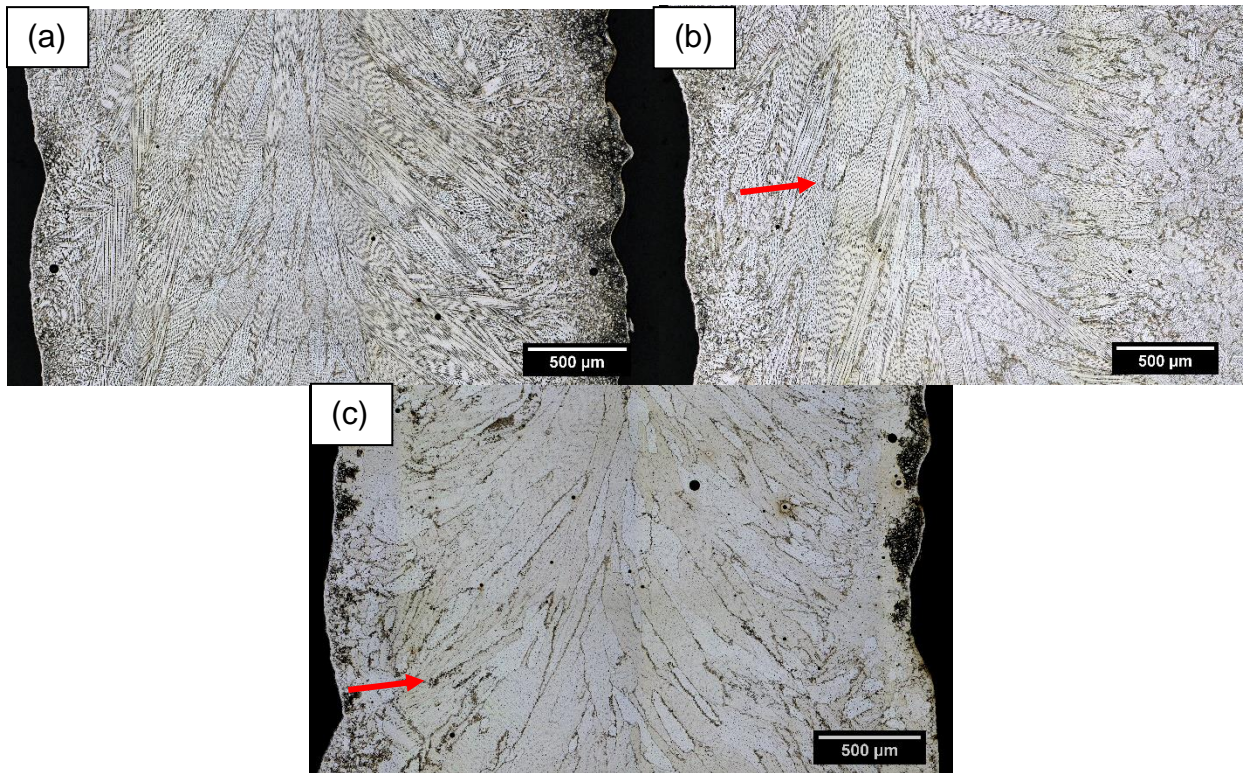


Fig. 6: Optical micrographs of DED NASA HR-1 after stress relief treatments at various temperatures for 1.5 hours. With increasing temperature, greater recovery was observed and the melt pool boundaries dissipated. (a) 1700°F, (b) 1750°F, (c) 1800°F. The red arrows indicate examples of the needle-like η -phase.

After stress relief, panel samples were subjected to a HIP cycle consistent with AM Ni-based superalloys including some variations on these standard cycles. The microstructure of thicker single-pass panels and multi-pass blocks after HIP is shown in Fig. 7. At both temperatures, an acceptable degree of recrystallization and significant twinning was observed. However, while most of the grains in the panels were equiaxed, several high aspect ratio grains were evident. Additionally, many grains in the material were larger than 300 μm in diameter. The grain size is attributed to the large melt pool dimensions in these samples. The higher temperature HIP was observed to have promoted more grain growth in the sample. In the panels at both temperatures, a difference in grain size in the panels is noticeable between the middle of the panel and the edges. Along the edges, much finer grains form compared to the middle of the sample. This effect appears from panels being a single pass and the cooling rate of the material during deposition. As the material cools, the middle of the sample takes much longer than the edges leading to larger grains in the middle.

The block was subjected to the lower temperature HIP cycle. In the block, large equiaxed grains were observed throughout with very few columnar grains. The general uniformity of the grains may be attributed to having multiple passes and different scan strategy from the panels. However, the top layer of the blocks did not appear to recrystallize resulting in large columnar grains remaining in the top 2-3 mm of the block. For some applications, using the larger melt pool width for faster deposition and shorter build times would be acceptable. This result may not be consequential though since the areas impacted by this sort of microstructure will be small and in regions where there are not large enough stresses to notice any anisotropy or difference in materials properties. Some of these regions may also be machined off as part of some post-processing procedure to clean surfaces for additional welding or other purposes. Based on the observations in both the panels and the block, the lower temperature was preferred as it exhibited acceptable amounts of recrystallization and grain growth for the given samples.

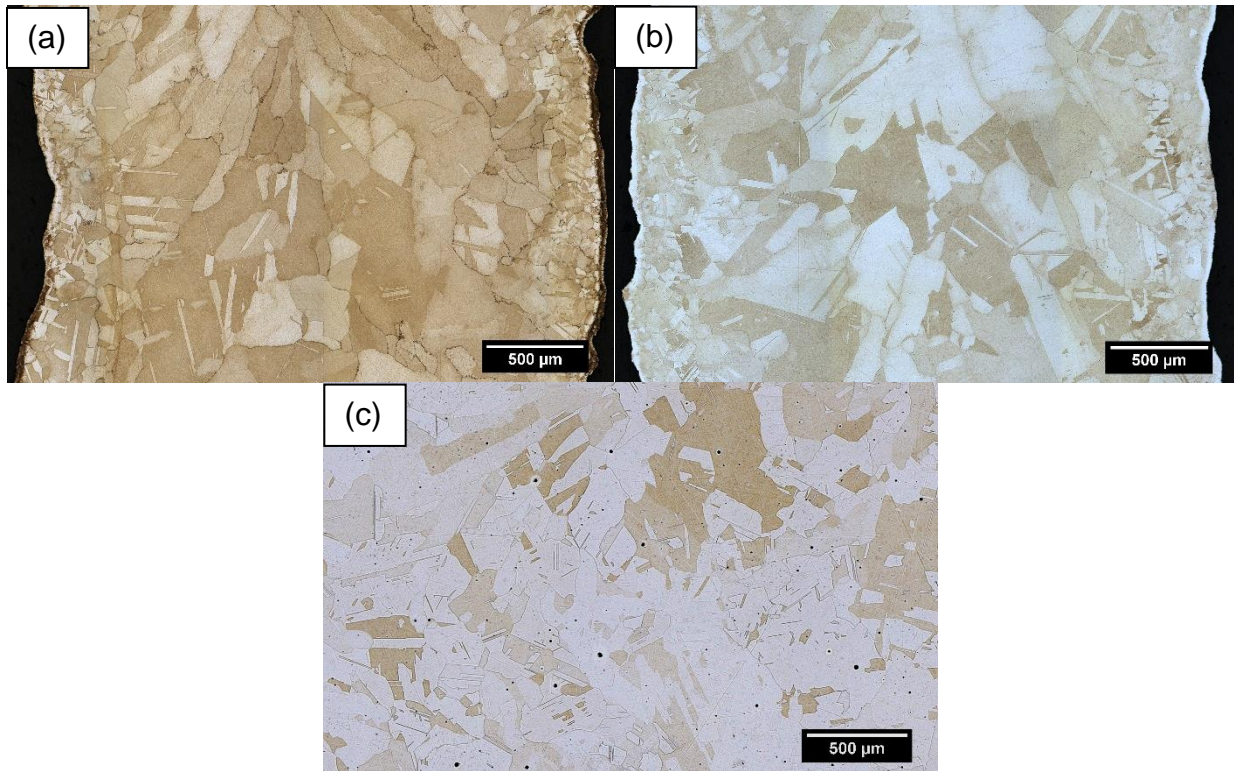


Fig. 7: Optical micrographs of DED NASA HR-1 after stress relief of 1800°F for 1.5h and hot isostatic pressing (HIP) of single pass panel samples (a, b) with increasing temperature and multiple-pass block at the common temperature (c).

At the end of the stress relief, the parts were slow cooled in order to allow for the most recovery. This is also observed in the HIP processing as the samples also undergo a slow cooling, due to the reduction in chamber pressure and temperature prior to opening the HIP. As a result, the formation of the needle-like η -phase was observed at the grain boundaries in the slowly cooled samples. The η -phase appears as needles or plates that highlight the grain boundaries in the early formation indicated in Fig. 6b and 6c and can develop into larger cells as shown in Fig. 8. This phase is brittle causing loss of ductility in the material, but can be eliminated by the solution treatment step [29]. After a solution treatment of 1800°F for 1h, the microstructure had been observed to be free of η -phase. However, when the samples had been standard aging treatment [30] (1325°F 16h), η -phase had developed in both the panel and block samples. The η -phase was observed to have primarily formed near the edges where the difference in grain size was observed, but it was seen to a lesser degree in the middle of panel and block samples after aging.

The presence of grain-boundary η phase (Ni_3Ti) in fully heat-treated DED NASA HR-1 samples is a serious concern as η -phase is brittle and has a negative impact on tensile ductility and HEE resistance. The η -phase can be eliminated by solution treatment at 1800 °F for 1 h, followed by water quench or forced air-cooling. However, η precipitation can occur in some areas after aging at 1325 °F/16h due to higher localized Ti segregation at grain boundaries. A TTP (Time-Temperature-Precipitation) diagram for η phase in DED NASA HR-1 superalloy is being developed at MSFC to provide guidelines for selecting appropriate aging temperatures for DED HR-1. The η -phase precipitation can be prevented by lowering the aging temperature (to 1300 °F or 1275 °F), but tensile strength will decline by approximately 5 - 10 %. In order to offset the strength drop when the material is aged at a lower temperature, the standard single-step aging treatment will be modified into a 2-step aging process. The 2-step aging process can strengthen the alloy by having secondary γ' precipitation during the 1st aging treatment (higher

temperature) and finer secondary or tertiary γ' precipitation during the 2nd step aging (lower temperature). By controlling the aging temperatures and duration, η precipitation can be prevented to obtain optimum tensile properties.

DED NASA HR-1 appears to have higher Ti segregation at grain boundaries that is not normally seen in the wrought NASA HR-1. The difference in Ti micro-segregation can be attributed to the difference in the solidification rates between DED and casting processes. The casting process has much slower cooling (solidification) rate that allows for prolonged cooling times in the castings, permitting larger and slow-to-diffuse elements (such as Ti) to disperse more homogeneously than DED parts. In addition, NASA HR-1 casting receives homogenization treatment at elevated temperatures for 25 hours. This condition, upon similar heat treatment, makes it less favorable for the precipitation of η -phase, since there are lower concentrations of Ti at grain boundaries. The η precipitation at grain boundaries can lead to lower strength for DED NASA HR-1 as η -consumes titanium and reduces γ' volume fraction.

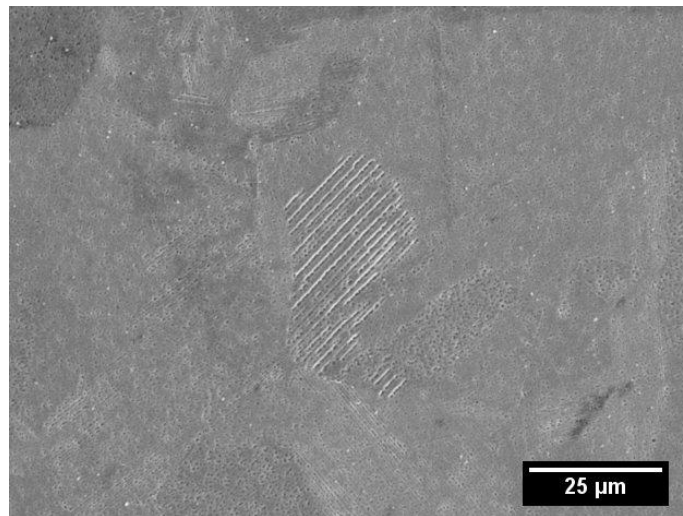


Fig. 8: SEM micrograph of the needle-like η -phase phase precipitate that can form in NASA HR-1.

SLM NASA HR-1 coupons were subjected to the recommended heat treatments established from the previous analysis of DED NASA HR-1. Fig. 9 shows the evolution of the microstructure for these coupons from the as built to HIP. As expected, columnar grains form in the as built, but the grains that form in SLM NASA HR-1 are noticeably finer than the DED samples. This is due to using smaller melt pool in the SLM coupons compared to the DED samples that were subjected to heat treatments. After stress relief (Fig. 9b), the melt pools were no longer visible and there was an acceptable amount of recrystallization indicating that the stress relief treatment works for both DED and SLM NASA HR-1, and after HIP (Fig. 9c), the microstructure was fully recrystallized with finer equiaxed grains than DED. The finer microstructure is expected to result in increased tensile strength in SLM material compared to DED.

Similar to DED, η -phase was observed to form near the grain boundaries after stress relief and HIP. While the solution and aging steps for SLM samples has not been examined, it is expected that the η -phase could still form after the standard aging step due to the rapid cooling rates in the SLM process. However, the finer microstructure found in SLM NASA HR-1 may help to suppress the formation of η -phase throughout the microstructure after aging as the Ti will be able to diffuse into grains more easily during the HIP/homogenization and solution treatments.

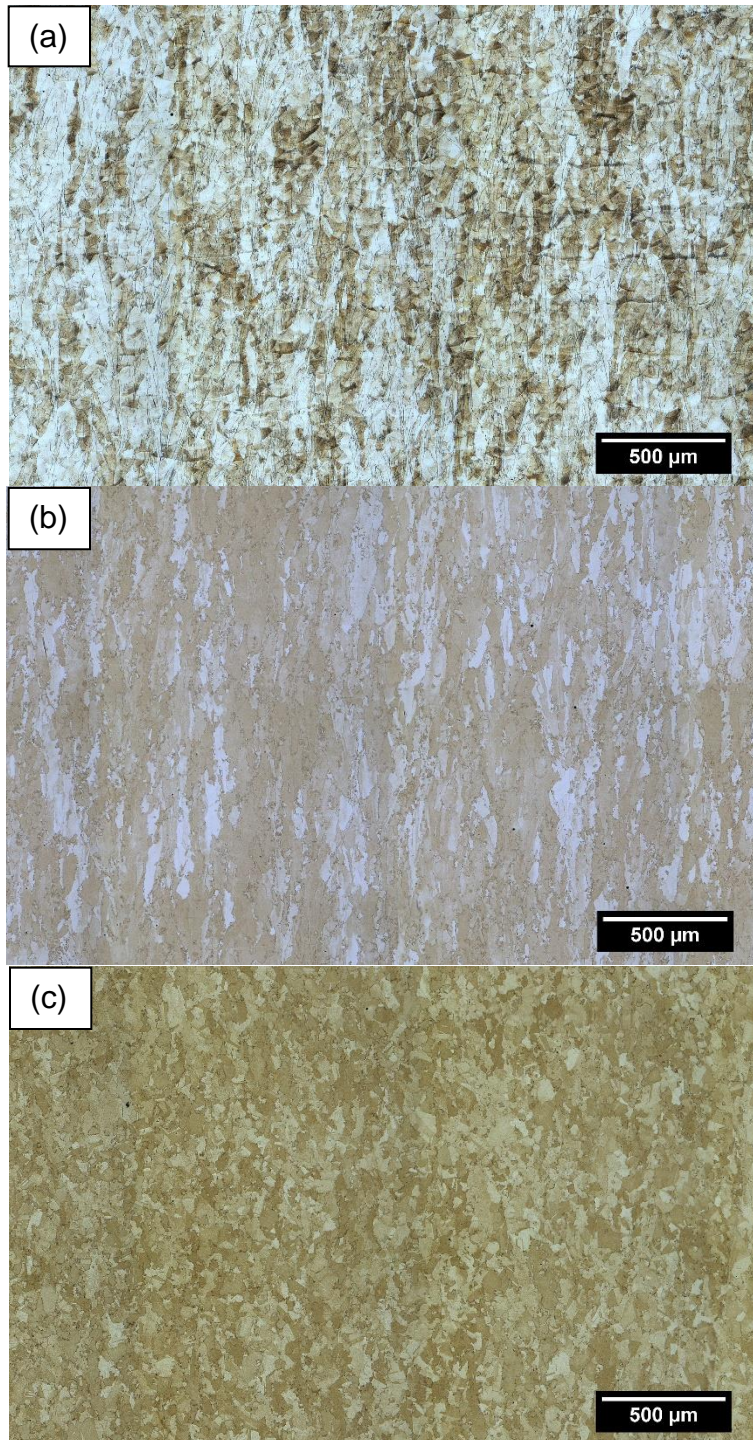


Fig. 9: Microstructure of L-PBF SLM through different stages of recommended heat treatment cycle. (a) As-Built, (b) Stress-Relieved, (c) HIP.

Vickers micro-hardness measurements were taken in the as-built, stress relieved, and HIP conditions for both DED and SLM NASA HR-1 samples. Additional measurements were taken after the recommended heat treatment with a full standard age for DED samples. At least 20 measurements were taken to produce an average HV shown in Table 3 and Fig. 10. These measurements aid the evaluation of the heat treatment by providing a quantitative measure that gives an indication of recrystallization, grain growth, and tensile properties [31]. The trend observed in the micro-hardness is an increase after stress

relief as the material recovers but is only starting to recrystallize. The micro-hardness in the 1800°F stress relief was also observed to be higher than the 1700°F treatment likely due to a greater degree of recovery. There is a drop in micro-hardness after HIP due to the recrystallization and grain growth in the material. For SLM, this drop is not very significant due to the finer grain size and limited growth after HIP compared to DED. After the full age in the DED material, some of the micro-hardness is recovered as more γ' precipitates and strengthens the material.

Table 3: Average Vickers micro-hardness measurements for DED and SLM NASA HR-1 in the various material conditions from as-built to fully aged.

Material Condition	Average Vickers Micro-hardness (HV)	
	DED	SLM
As-Built	199.8	260
Stress Relief 1700°F	332.6	335.1
Stress Relief 1800°F	354.6	371.8
HIP Lower T	312.2	362.7
HIP Higher T	292.5	357.1
Full Standard Age	328.5	-

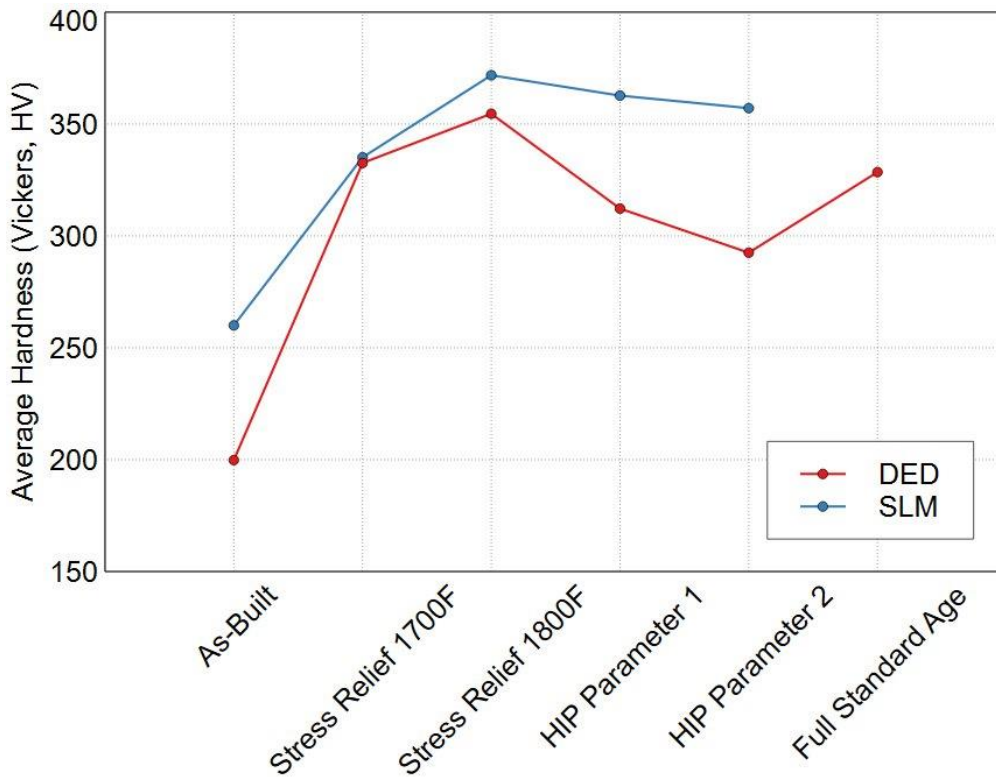


Fig. 10: Plot of Average Vickers micro-hardness measurements for DED and SLM NASA HR-1

FUTURE WORK

Further characterization of additively manufactured NASA HR-1 is currently being completed and planned to continue through several NASA projects. Once the final aging heat treatment step has been developed, the mechanical properties will be tested at room temperature, elevated temperature testing, and in a hydrogen to determine its full HEE resistance. The weldability of AM NASA HR-1 will also be examined through a series of qualitative and quantitative welding trials primarily focused on the DED material initially.

During the development of NASA HR-1 for AM, the powder composition specification has been revised using PHACOMP analysis. The purpose of these revisions was to optimize the stability and properties, specific to the regen-cooled nozzle application as described above. While strength is important for the application, there were other material properties such as conductivity and fatigue could be improved to optimize the material further for components. Currently, samples based on the first two revisions of the NASA HR-1 powder specification have been examined, but a third revision has been made primarily in an effort to improve the thermal conductivity of NASA HR-1. The rationale for this revision was that by decreasing the volume percentage of γ' and suppressing the formation of η -phase, there will be an improvement to thermal conductivity, ductility, HEE resistance, and LCF life at the expense of yield strength.

Table 4: Revisions of AM powder composition specifications for NASA HR-1.

AM NASA HR-1 Powder Composition Revisions (Wt%)

	R1	R2	R3
Fe	Bal	Bal	Bal
Ni	33.7 – 34.3	33.0 – 35.0	33.7 – 34.3
Co	3.1 – 3.5	3.0 – 3.5	3.6 – 4.0
Cr	15.2 – 15.7	14.0 – 16.0	14.3 – 14.9
Mo	2.0 – 2.4	1.8 – 2.2	1.6 – 2.0
V	0.3 – 0.34	0.3 – 0.5	0.28 – 0.32
W	1.9 – 2.3	1.5 – 2.0	1.4 – 1.8
Ti	2.3 – 2.7	2.4 – 2.8	2.2 – 2.6
Al	0.23 – 0.3	0.1 – 0.4	0.23 – 0.27

NASA is continuing to fabricate a series of demonstrator components using the NASA HR-1 in parallel with the materials development and characterization. This hardware is to strategize build approach, toolpaths, and determine appropriate design geometry to meet full design intent and requirements. Some of these parts will undergo evaluation through flow and proof testing in addition to hot-fire testing to evaluate the process and material performance fully in a relevant environment. NASA is currently fabricating several 2K-lbf and 35K-lbf-class integral channels in DED NASA HR-1. Additionally, several thicker-wall components including nozzle liners, manifolds, and flanges are being fabricated at several vendors in DED NASA HR-1 and L-PBF NASA HR-1.



Fig. 11: Examples of integral-channel nozzles and thick-wall mid-scale nozzle, DED NASA HR-1.

SUMMARY AND CONCLUSIONS

NASA HR-1 is potentially an enabling material for high-pressure, high-temperature hydrogen applications. Previous manufacturing and processing methods made the use of NASA HR-1 impractical for cost and schedule reasons. However, with the progress made with various additive manufacturing techniques, NASA HR-1 has the potential to be affordably manufactured for use in propulsion applications, such as integral channel wall nozzles and other components as a forging and casting replacement. NASA HR-1 has been shown to be a printable alloy in both blown powder DED and SLM processes, and a desirable microstructure has been shown to be attainable through the heat treatment development discussed.

In blown powder DED, the melt pool (spot size) and scan pattern were shown to have an impact on the grain size of as-built and heat treated samples. As the melt pool size increases, the grain size was observed to increase in the sample, and the grain size was also shown to break up when the deposition method was changed. While most of an optimal heat treatment has been developed, the final aging step of AM NASA HR-1 needs to be adjusted in order to avoid formation of η -phase precipitates in order to attain the desired mechanical properties and optimal HEE resistance.

NASA is continuing to develop AM NASA HR-1 DED and SLM material specimens to fully characterize during heat treatments in addition to completion of mechanical testing. Several components are being fabricated using AM NASA HR-1 and planned to complete hot-fire testing. Additional data will be made available including material properties and lessons learned during development using these processes as funded under the Liquid Engines Office (LEO) IRAD and Rapid Analysis and Manufacturing Propulsion Technology (RAMPT) project.

- [1] Chen, P. S., Panda, B., and Bhat, B. N. NASA HR-1, A New Hydrogen Resistant Fe-Ni Base Superalloy. 1996.
- [2] Thompson, A. W., and Brooks, J. A. "Hydrogen Performance of Precipitation-Strengthened Stainless Steels Based on A-286." *Metallurgical Transactions A*, Vol. 6, No. 7, 1975, p. 1431. doi:10.1007/BF02641935.
- [3] Smugeresky, J. E. "Effect of Hydrogen on the Mechanical Properties of Iron-Base Superalloys." *Metallurgical Transactions A*, Vol. 8, No. 8, 1977, pp. 1283–1289. doi:10.1007/BF02643843.
- [4] Thompson, A. W. "Hydrogen-Induced Ductility Loss in Commercial Precipitation-Strengthened Stainless Steel." *Met. Trans.*, Vol. 7A, 1976, pp. 315–318.
- [5] Decker, R. F. "Strengthening Mechanisms in Nickel-Base Superalloys." *Steel Strengthening Mechanisms Symposium, Zurich, Switzerland, May 5 and 6, 1969*, 1969, pp. 1–23.
- [6] Raynor, D., and Silcock, J. M. "Strengthening Mechanisms in Γ' Precipitating Alloys." *Metal Science Journal*, Vol. 4, No. 1, 1970, pp. 121–130. doi:10.1179/msc.1970.4.1.121.
- [7] Havalda, A. "Influence of Tungsten on the γ to η Transformation and Carbide Reactions in Nickel-Based Superalloys." *ASM (Amer. Soc. Metals), Trans. Quart.*, No. 62, 1969, pp. 581–589.
- [8] Morinaga, M., Yukawa, N., Ezaki, H., and Adachi, H. "Solid Solubilities in Transition-Metal-Based f.c.c. Alloys." *Philosophical Magazine A*, Vol. 51, No. 2, 1985, pp. 223–246. doi:10.1080/01418610.1985.12069159.
- [9] Morinaga, M., Murata, Y., and Yukawa, H. Recent Progress in Molecular Orbital Approach to Alloy Design. 2004.
- [10] Morinaga, M., and Yukawa, H. "Alloy Design with the Aid of Molecular Orbital Method." *Bulletin of Materials Science*, 1997. doi:10.1007/BF02747420.
- [11] Moody, N. R., Brooks, J. A., and Thompson, A. W. Development of JBK-75 for Service in High Pressure Hydrogen Environments: The Role of Microstructure. 1992.
- [12] Gradl, P. R., Protz, C., and Wammen, T. Additive Manufacturing Development and Hot-Fire Testing Directed Energy Deposition Inconel 625 and JBK-75 Alloys. No. 2019, 2019, pp. 1–20.
- [13] Gradl, P., Mireles, O., and Andrews, N. "Introduction to Additive Manufacturing for Propulsion Systems Additive Manufacture Is Real" 2019.
- [14] Anderson, R., Terrell, J., Schneider, J., Thompson, S., and Gradl, P. "Characteristics of Bi-Metallic Interfaces Formed During Direct Energy Deposition Additive Manufacturing Processing." *Metallurgical and Materials Transactions B: Process Metallurgy and Materials Processing Science*,

- Vol. 50, No. 4, 2019, pp. 1921–1930. doi:10.1007/s11663-019-01612-1.
- [15] Onuike, B., Heer, B., and Bandyopadhyay, A. “Additive Manufacturing of Inconel 718—Copper Alloy Bimetallic Structure Using Laser Engineered Net Shaping (LENS™).” *Additive Manufacturing*, 2018. doi:10.1016/j.addma.2018.02.007.
- [16] Bandyopadhyay, A., and Heer, B. Additive Manufacturing of Multi-Material Structures. *Materials Science and Engineering R: Reports*.
- [17] Hauser, C. “Additive Manufacturing Seminar: Blown Powder Activities.” *TWI Materials and Joining Technologies*. Retrieved from: www.twi-global.com/resources, 2015.
- [18] Karczewski, K., Dąbrowska, M., Ziętała, M., and Polański, M. “Fe-Al Thin Walls Manufactured by Laser Engineered Net Shaping.” *Journal of Alloys and Compounds*, 2017. doi:10.1016/j.jallcom.2016.12.034.
- [19] Chan, K. S., Koike, M., Mason, R. L., and Okabe, T. “Fatigue Life of Titanium Alloys Fabricated by Additive Layer Manufacturing Techniques for Dental Implants.” *Metallurgical and Materials Transactions A: Physical Metallurgy and Materials Science*, 2013. doi:10.1007/s11661-012-1470-4.
- [20] DebRoy, T., Wei, H. L., Zuback, J. S., Mukherjee, T., Elmer, J. W., Milewski, J. O., Beese, A. M., Wilson-Heid, A., De, A., and Zhang, W. Additive Manufacturing of Metallic Components – Process, Structure and Properties. *Progress in Materials Science*.
- [21] Sames, W. J., List, F. A., Pannala, S., Dehoff, R. R., and Babu, S. S. The Metallurgy and Processing Science of Metal Additive Manufacturing. *International Materials Reviews*.
- [22] Gradl, P. R., Protz, C., Ellis, D. L., and Greene, S. E. Progress in Additively Manufactured Copper-Alloy GRCop-84, GRCop-42, and Bimetallic Combustion Chambers for Liquid Rocket Engines. *IAC-19.C4.3.5x52514*.
- [23] Gradl, P. R., Greene, S. E., Protz, C., Bullard, B., Buzzell, J., Garcia, C., Wood, J., Cooper, K., Hulka, J., and Osborne, R. Additive Manufacturing of Liquid Rocket Engine Combustion Devices: A Summary of Process Developments and Hot-Fire Testing Results. 2018.
- [24] Bremen, S., Meiners, W., and Diatlov, A. “Selective Laser Melting.” *Laser Technik Journal*, 2012. doi:10.1002/latj.201290018.
- [25] ASTM International. “Standard for Additive Manufacturing – Post Processing Methods – Standard Specification for Thermal Post-Processing Metal Parts Made Via Powder Bed Fusion.” *ASTM Standards*, 2018, p. 3. doi:10.1520/F3301-18.
- [26] Popovich, V. A., Borisov, E. V., Popovich, A. A., Sufiiarov, V. S., Masaylo, D. V., and Alzina, L. “Functionally Graded Inconel 718 Processed by Additive Manufacturing: Crystallographic Texture, Anisotropy of Microstructure and Mechanical Properties.” *Materials and Design*, Vol. 114, 2017, pp. 441–449. doi:10.1016/j.matdes.2016.10.075.
- [27] Kok, Y., Tan, X. P., Wang, P., Nai, M. L. S., Loh, N. H., Liu, E., and Tor, S. B. “Anisotropy and Heterogeneity of Microstructure and Mechanical Properties in Metal Additive Manufacturing: A Critical Review.” *Materials and Design*, 2018. doi:10.1016/j.matdes.2017.11.021.
- [28] Yan, F., Xiong, W., and Faierson, E. J. “Grain Structure Control of Additively Manufactured Metallic Materials.” *Materials*, Vol. 10, No. 11, 2017, p. 1260. doi:10.3390/ma10111260.
- [29] Li, C. W., Yeh, A. C., Chen, C. S., and Wang, W. R. “Hot Ductility Loss in a Fe-Ni-Based Superalloy.” *Metals*, Vol. 5, No. 4, 2015, pp. 2428–2434. doi:10.3390/met5042428.
- [30] Chen, P., and Mitchell, M. NASA HR-1. August.
- [31] Callister, W. D., and Rethwisch, D. G. *Fundamentals of Materials Science and Engineering: An Integrated Approach*. Wiley, 2009.